Development of lane-precise “Ground Truth” maps for the objective Quality Assessment of automated driving functions

Dipl.-Ing. (FH) **S. Keidler**[1], M. Sc. **D. Schneider**[1,2], M. Sc. **J. Haselberger**[1], M. Sc. **K. Mayannavar**[1], Prof. **B. Schick**[1]

[1]University of Applied Science Kempten, Kempten
[2]AVL Deutschland GmbH, Karlsruhe

Abstract

The focus of this publication is on the development of lane-precise “Ground Truth” (GT) maps for the objective quality evaluation of automated driving functions. Therefore, attention is paid to the proper measurement of road geometry. The road geometry forms the basic layer of the HD maps. A new map format Curved Regular Objects (CRO) is developed, which is based on the idea of OpenCRG®. For the evaluation of current Advanced Driver Assistance Systems (ADAS) an accurate High Definition (HD) maps as GT are necessary. This makes it possible to locate the high precision vehicle position and motion with centimeter accuracy. The aim is to achieve maximum accuracy of the absolute 3D positions when measuring lanes. This method for the generation of highly accurate GT maps promises an absolute accuracy of $< \pm 0.05$ m. Various research activities benefit from the exact street reference at the *Kempten University of Applied Sciences (UAS Kempten)* in the *Adrive Living Lab*. First of all, the publication deals with the current Lane Keeping Assistant Systems (LKAS). The accuracy of the vehicle’s localization on the GT map and an objective evaluation of the LKAS is shown. In addition, the CRO data is used as a virtual sensor for the steering assistant in real time. Another application is the Visual Range Finder (VRF), which requires less computation power by using the CRO data. In addition, a current LKAS camera sensor performance is evaluated using CRO maps.

1 Introduction

Advanced Driver Assistance Systems (ADAS) and Automated Driving (AD) are becoming increasingly important in the automotive industry. For customer satisfaction [1] and brand differentiation of vehicle manufactures, objective evaluation of driving characteristics and corresponding target definitions of automated driving functions are essential [2]. Test standards such as ISO [3], NCAP [4] or UN/ECE [5] cannot fully reflect customer experience and realistic driving situations [6]. Even today's test tracks cannot offer the variance of the real environment. Road description parameters such as curve radius, curvature, slope, road markings, road bank angle and road bank angle gradient have a considerable influence on the driving dynamics and therefore on the driving characteristics of automated driving functions of the lateral vehicle control [2] [7].

2 Motivation and concept

Transferred to the automated lateral control, the following applies: Knowledge of road parameters such as road markings and topology must be well known and acquired. This results in evaluation of vehicle reaction. Together with *Porsche AG* and *MdynamiX AG*, the *Kempten University of Applied Sciences (UAS Kempten)* has developed an objective evaluation methodology for this purpose [2]. In addition, intensive research on Ground Truth (GT) methods is being carried out at the *UAS Kempten*. Like all sensors, vehicle environment sensors such as camera, RADAR or LiDAR are faulty and not available or sufficiently accurate in all situations. This can have a significant influence on the driving performance. For example, the camera may not be able to reproduce the curvature of curves adequately, which can have an effect on the lane departure control [8]. This results in uncertainties. The driving characteristics result from a limited performance of the sensors, trajectories, controllers, actuators or the moderate response of the vehicle [3]. In order to analyze this chain, a significantly more accurate reference measurement method must be used: the Ground Truth (GT) [7]. The approach was to integrate a highly accurate measured vehicle position and movement into highly accurate digital GT maps (Figure 1).

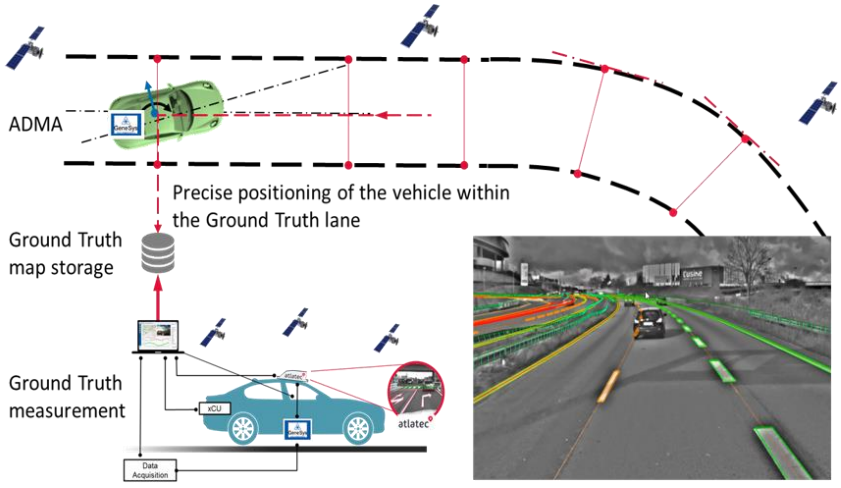

Figure 1: GT measurement methodology referring to [2].

Atlatec GmbH has developed a method to measure roads to a high accuracy. To date, sections of country roads, federal highways and motorways have been digitized over a distance of more than 130 km. A newly developed road description format Curved Regular Objects (CRO), based on the OpenCRG® [9], describes the roadway with all relevant features in a regular grid. An ADMA G-Pro+ from *GeneSys Elektronik GmbH* (Inertia Measurement Unit, IMU) was used for position and motion measurement [10]. The current results show that it is possible to locate the vehicle to an accuracy of a few centimeters in the digital GT maps in real time. This publication presents the procedure of generating GT maps. In addition, the new possibilities of proper evaluation the vehicle movement are shown using the example of a Lane Keeping Assistant System (LKAS).

3 State of the art

AD requires map data that differs significantly from current navigation systems. The driver uses a digital map designed for the route planning. In the future, ADAS will request more comprehensive information about the roads. Therefore, the digital map must be understood by machines and no longer primarily by humans [11]. This is called High Definition (HD) maps. Many companies such as *HERE Global B.V.* [12], *TomTom N.V.* [13] or *Robert Bosch GmbH* [14] are preparing their maps for AD. HD maps are built as layer-based. The aim is to meet the requirements of AD for the HD map layers (Figure 2) [13].

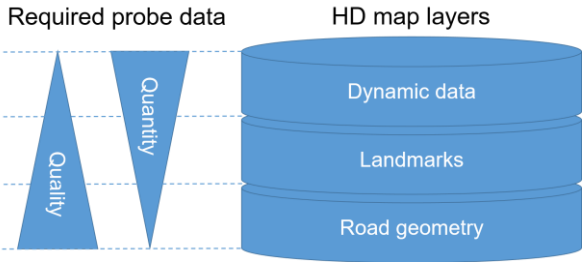

Figure 2: Requirements of autonomous driving for HD map layers referring to [13].

Representation of road geometry requires the highest accuracy. At the same time, the amount of road geometry data is reduced to a minimum. Landmarks describe static road objects with increasing amount of data and high accuracy. Dynamic data have a lower quality, but a high quantity [13].

3.1 Road geometry for automated driving functions

Road geometry contains absolute 3D positions of the roadway and information about the road markings and lanes. The ground layer forms the basis of the HD map. High quality of road data acquisition and a reduction of the amount of data to only that which essential is necessary. The HD Lane Model by *HERE Global B.V.* [12] and the 3D Lane Map Layer by *TomTom N.V.* [13] describe the road geometry. The OpenCRG® data format describes the road geometry in position and height [9]. Together with the OpenDRIVE® data, road surfaces can be stored within an accuracy of centimeters [15]. This data is required to evaluate current LKAS [2].

3.2 Landmarks for real-time localization

Landmarks are static road objects such as traffic signs, tunnels, bridges, houses, traffic lights and much more. The absolute 3D position and typical properties of the road objects are stored in a separate layer. The landmarks are used during AD for the real-time localization of the ego vehicle in the HD maps [2]. The HD Localization Model from *HERE Global B.V.* [12] and the RoadDNA from *TomTom N.V.* [11] provide landmark data. The Radar Road Signature method from *Robert Bosch GmbH* [14] measures landmarks and stores this information for AD with high accuracy.

3.3 Dynamic data for real-time map updates

The dynamic data refer to changes in road geometry or landmarks [13]. The current traffic situation with traffic jam ends or sudden weather changes also influence the traffic flow. ADAS need knowledge about changing environmental events. *HERE Global B.V.*'s self-healing maps use sensors in series vehicles and satellite images to update and change data. New technologies such as Artificial Intelligence (AI) and Deep Learning (DL) are used for this purpose [12]. Based on this knowledge a new road description format CRO will be developed. The method for the development of lane-precise GT maps should allow an absolute accuracy of < ± 0.05 m.

4 Methodology

This chapter introduces the method for creating lane-precise CRO maps. First, the procedure is simplified (Figure 3).

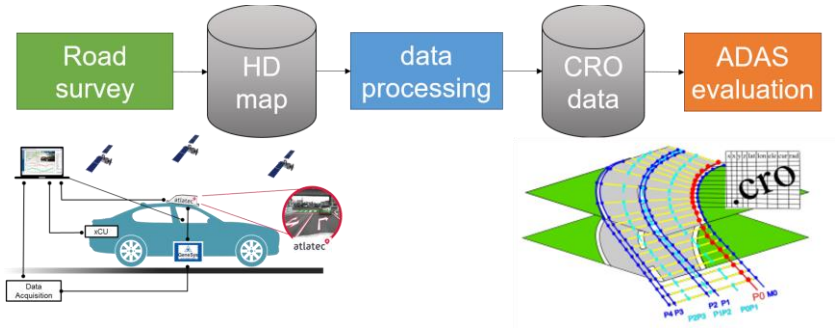

Figure 3: Procedure for the development of lane-precise GT maps (CRO)

Road survey data from *Atlatec GmbH* are recorded with a stereo camera and an ADMA G-Pro+ with RTK-GPS (SAPOS HEPS) from *GeneSys Elektronik GmbH* [10]. The digital HD map from *Atlatec GmbH* is provided in OpenStreetMap (OSM) format. The data is structured and interpolated. According to the concept of OpenCRO®, the data will be stored in a regular grid [9].

4.1 CRO map layer

The basic concept of the CRO map is a regular grid. The geographical absolute positions of the lanes are shown in CRO layer 0 (Figure 4). The reference line P0 is the inner edge of the right-hand edge of the road (red polyline). The grid is constructed on this basis. The

orthogonal yellow lines divide the roadway into individual segments. The intersections with the other polylines (blue and turquoise) result in further geographical grid points. The names of all other polylines are based on the direction of travel, increasing to the left P1, P2, P3, P4, and to the right M0. The virtual turquoise polylines P0P1 and P2P3 describe the center lines of each lane.

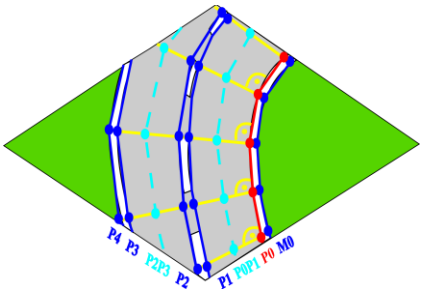

Figure 4: CRO layer 0: Geographical lane-precise GT grid.

Based on the CRO layer 0, the CRO layer 1 is developed (Figure 5). Individual road description parameters allow a classification of the roadway. These include parameters such as gradient, curve radius, curvature, azimuth angle, road width and road bank angle.

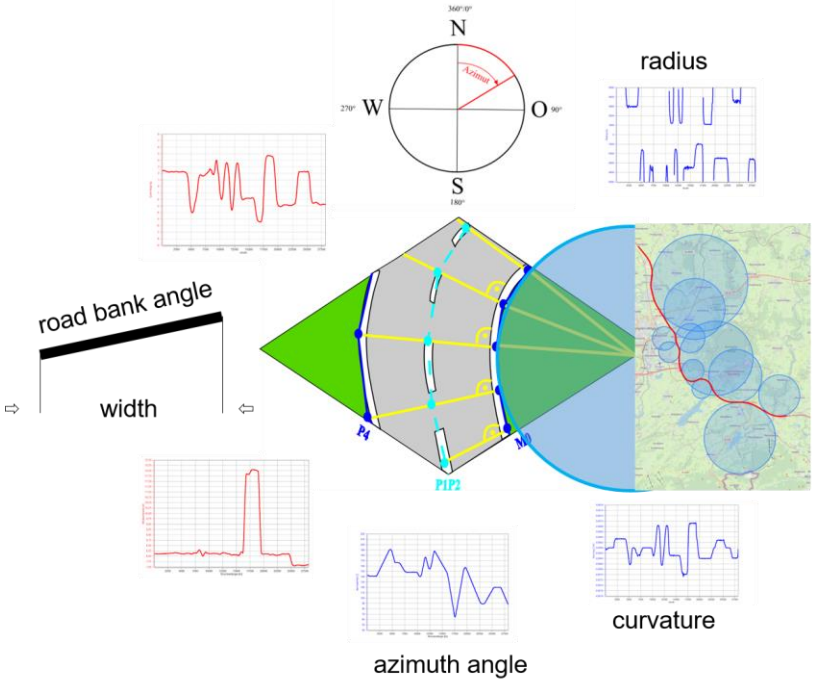

Figure 5: CRO layer 1: Roadway with road description parameters.

The CRO layer 2 describes landmarks such as street signs (Figure 6). The landmarks are

stored relative to line P0, which maintains the reference to the regular grid. Each landmark has a unique fingerprint as a key descriptor array.

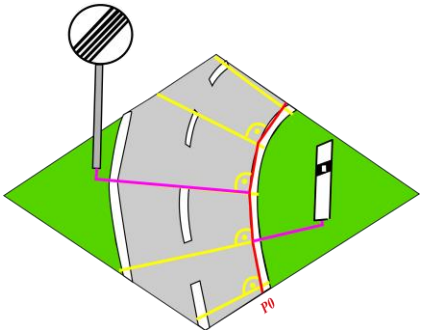

Figure 6: CRO layer 2: Landmarks with reference to the regular grid.

The individual CRO layers can be extended according to requirements, and can be assigned via unique indexing. This simplifies the use of individual parameters under real-time conditions.

4.2 Calculation of the regular grid

Intermediate steps are necessary for the calculation of the orthogonal grid. First the road survey data is read in. The survey data is then assigned to individual polylines according to the direction of travel. Finally, the survey data is interpolated after a variable increment and the orthogonal grid is calculated.

The road survey data contain absolute geographic coordinates and are not assigned to individual lane markings (figure 7).

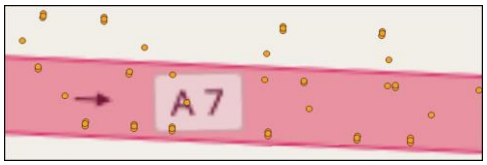

Figure 7: Parsing the road survey data.

In the next step, the DGPS coordinates are assigned to the polylines (Figure 4). It is important to store the DGPS coordinates in individual polylines according to the direction of travel. An automated calculation routine detects the corresponding DGPS coordinates, and sorts and saves them, which results in the polylines M0, P0, P1, P2, P3 and P4 (Figure 8).

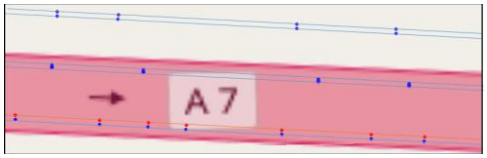

Figure 8: Assignment of road survey data to individual polylines.

The reference line P0 is interpolated and stored with a resolution of 1 meter between the DGPS coordinates (adjustable). The other polylines are perpendicular aligned to the reference line P0 (Figure 9).

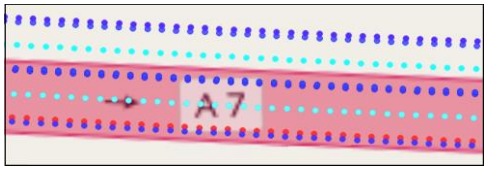

Figure 9: Interpolation and orthogonal alignment of polylines to the grid.

4.3 Validation of the regular grid accuracy

The accuracy of the CRO grid can be determined on the basis of the survey data from *Atlatec GmbH*. The error in longitudinal and lateral direction is calculated for this purpose. Therefore the methodology for validating the regular grid accuracy is described (Figure 10).

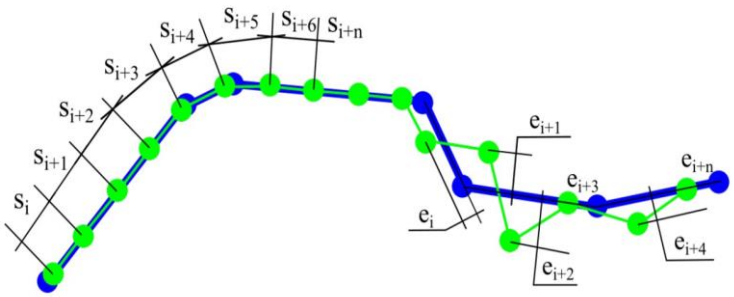

Figure 10: Validating the accuracy of the CRO grid.

The blue measuring points are the raw survey data. The green grid points have a regular distance and are the CRO data. The left part of the figure describes the calculation of the longitudinal error. The sum of all relative distances between the CRO coordinates is determined. The determination of the lateral error is shown on the right. The sum of perpendicular distances from the CRO data to the raw survey data is calculated. A polyline with 28190 CRO coordinates is used as an example. The raw survey data have a number of 4391 DGPS points. Both errors of the CRO data are calculated (Table 1).

method	number	mean value m	standard deviation m	confidence range m
Longitudinal error	28190	1.0006	0.0006	± 0.0004
Lateral error	28190	0.0009	0.0238	± 0.0087

Table 1: Longitudinal and lateral errors of the CRO data.

In longitudinal direction the CRO grid is 1.001 m ± 0.001 m accurate. The CRO grid data have a lateral error to the raw survey data of 0.001 m ± 0.01 m.

5 Localization accuracy of a vehicle position in the CRO maps

The localization of a measuring vehicle in HD maps is a central topic in the field of AD. Therefore, this chapter deals with the accuracy of locating a vehicle position in the CRO maps (Figure 11).

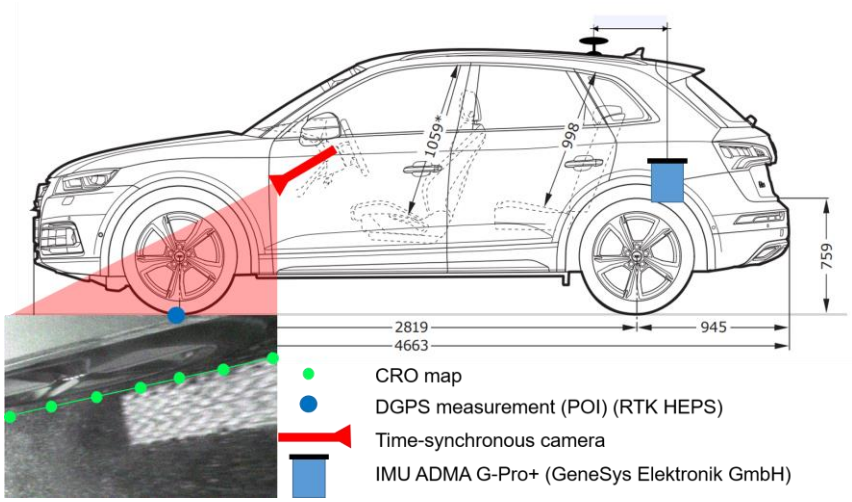

Figure 11: Measurement setup for determining the localization accuracy in the CRO maps.

The IMU ADMA G-Pro+ from *GeneSys Elektronik GmbH* and a DGPS measuring unit (blue) is illustrated. The relative, perpendicular distance calculation is determined from the DGPS position between the outer edge of the right front tire (blue) and the CRO maps (green). In addition, a time-synchronous camera is installed with a view to the right front tire and the road surface (red). 151 lane markings are crossed. The synchronous video frame identifies the time when the vehicle crosses the lane. The expected relative perpendicular distance between thevehicle and the road mark is zero. The orthogonal distance between vehicle and CRO map is calculated (Table 2).

DGPS status	number	mean value m	standard deviation m	confidence range m
8	52	−0.066	0.062	± 0.026
4	99	−0.258	0.373	± 0.113

Table 2: Localization accuracy in the CRO maps.

The DGPS status is determined depending on the standard deviation of the DGPS measurement. The DGPS Status 8 corresponds to a standard deviation of the DGPS measurement of less than 0.02 m. The perpendicular distances of 52 measuring points give an average value of −0.066 m with a standard deviation of 0.062 m. The orthogonal distance to the CRO map is 99.7% within the confidence range of −0.066 m ± 0.026 m. The DGPS Status 4 corresponds to a standard deviation of the DGPS measurement of 0.161 m. The 99 measuring points result in a perpendicular distance to the CRO maps of −0.258 m ± 0.113 m. The localization accuracy of −0.066 m ± 0.026 m at DGPS status 8 guarantees the required absolute accuracy of the vehicle position of ± 0.05 m using the CRO maps.

6 Evaluation of lane keeping assistant systems

Behavior driven development of ADAS becomes more and more important especially for ADAS of level 3 and higher. To validate and verify the degree of compliance, objective key performance indicators (KPIs) as indicators for systems' performance are developed and applied by the *UAS Kempten* [10]. To evaluate lateral controlling ADAS, highly precise maps and digital twins are key enabler. High fidelity GT maps are used in post processing to calculate position-based KPIs after relocalization of the vehicle under test (VUT) within the lane [10]. The identical maps can also be used as "virtual sensors". To localize the VUT, an RTK-GPS (SAPOS HEPS), combined with *GeneSys Elektronik GmbH* ADMA G-Pro+, is used.

6.1 Spatial calculation

To calculate the distance between VUT and a particular/specified target line, the structured CRO format is used. Due to the orthogonal grid, time consumption search-algorithms are reduced to a minimum. After an initial point-search for the corresponding grid-point to VUT's GPS-point, the following grid points are prefetched based on a heuristic selection. To get the minimal distance between VUT's position and regular grid data, the so-called "perpendicular footpoint method" is used. Due to world-coordinates of the CRO data, the distance is calculated

in absolute coordinates using either Haversine or Vincenty's formula [16], [17]. The foresign of each point is set by an internal definition, whereas points sinistral the target line are positive. For a simplified flowchart of the entire process (Figure 12).

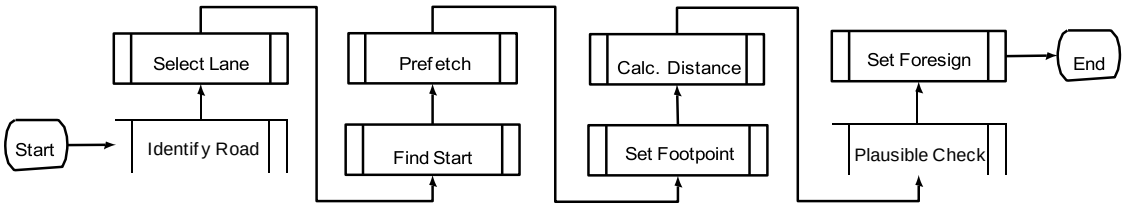

Figure 12: Schematic flowchart to obtain distance to target line.

6.2 Reference signals

Road-attributes such as *curvature* can be used to calculate reference-signals such as reference lateral acceleration ($a_{y,ref}$) and reference yaw rate ($\dot{\Psi}_{ref}$).

The reference lateral acceleration is required to execute the upcoming UN/ECE R79 assessment [5]. For instance, the "maximum lateral acceleration test" should be performed on a road-velocity-combination, where a higher lateral acceleration occurs than a specified lateral acceleration ($a_{y,s,max}$) + 0.3 m/s^2. In this way $a_{y,s,max}$ is defined by original equipment manufacturer (OEM) (or max. 3 m/s^2) [5], whereas the "lane keeping functional test" (LKFT) is only valid if the lateral acceleration during the measurement is between 80 and 90% of $a_{y,s,max}$. To ensure that the conditions are fulfilled the maps can be used as a virtual sensor to ensure the reference accelerations follow the road with a defined/known velocity. An equation for the calculation of the acceleration is given below.

$$a_{y,ref} = \frac{v_x^2}{r} = v_x^2 * curv \tag{1}$$

Segments on public roads are classified (blue) and a test plan can be prepared in more detail. The attribute *curvature* is also used to compute a reference yaw rate ($\dot{\Psi}_{ref}$) based on VUT's longitudinal velocity (Equation 2). With respect to the computation effort, a curvature is used instead of a radius since the multiplication is less time consuming than the division.

$$\dot{\Psi}_{ref} = \frac{v^x}{r} = v^x * curv \tag{2}$$

6.3 Key Performance Indicators

The reference yaw rate can be used to calculate a difference yaw rate between VUT's rate and GT (Equation 3).

$$\dot{\Psi}_{diff} = \dot{\Psi}_{ref} - \dot{\Psi}_{VUT} \tag{3}$$

The difference yaw rate represents the pre-cornering behavior of the VUT. I is calculated as difference between the yaw rate, which is required to follow the lane on given trajectory (center of the lane or racing line) and VUT's yaw rate. For instance, the center of the lane is the target trajectory of the LKAS (type 2) [10]. If required, the target line can be replaced with every parameterisable trajectory. To follow the target trajectory in a comfortable way (less lateral acceleration and jerk), the LKAS controller has to slur/blur the transition part from straight road segments into curved road segments. Thus, the difference yaw rate (given in figure 13(b)) directly before curve-entrance shall be greater than within the curve. By analyzing the size of peaks and amplitude, objective KPIs are provided. These KPIs are also used to benchmark vehicle's behavior and compare them to other VUTs, if single test drives were conducted on identical roads. Figure 13(a) shows the signals of the reference yaw rate and VUT's yaw rate at a specific road segment.

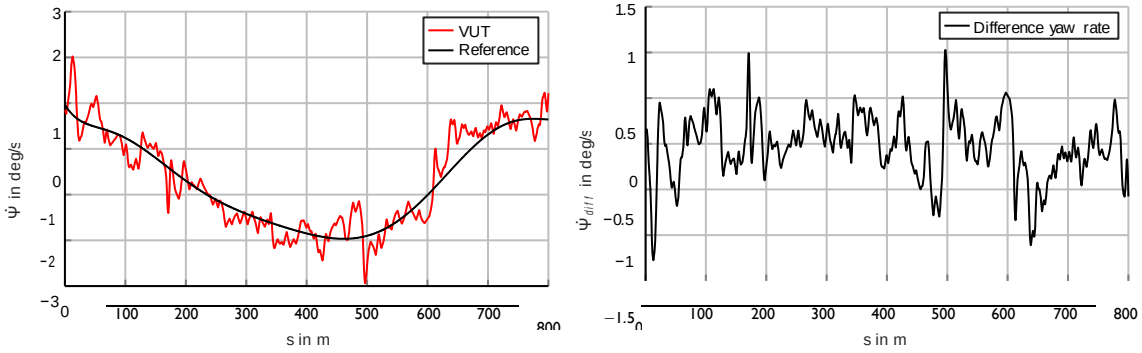

(a) Yaw rates (GT and VUT). (b) Difference yaw rate.

Figure 13: Yaw rate calculated and measured (13(a)) and difference yaw rate of each (13(b)).

The measured yaw rate is defined as the rate (derivation of the angle) between VUT and global north. The *GeneSys Elektronik GmbH* ADMA provide a signal with a resolution of 0.005° and

an accuracy of 0.05° [18].

By calculating the distance between VUT and target line (distance to target line, D2TL)(Figure 14), the entire system performance can be evaluated. The distances between VUT's front edges and line markings are calculated in parallel. By deriving the lateral displacement, the so-called drift velocity is calculated. However, this signal returns important KPIs as for instance general positioning offsets and predictability. Performing a Fast Fourier transform, the drift frequency is approximated in frequency domain as indicator for motion sickness [19], [20].

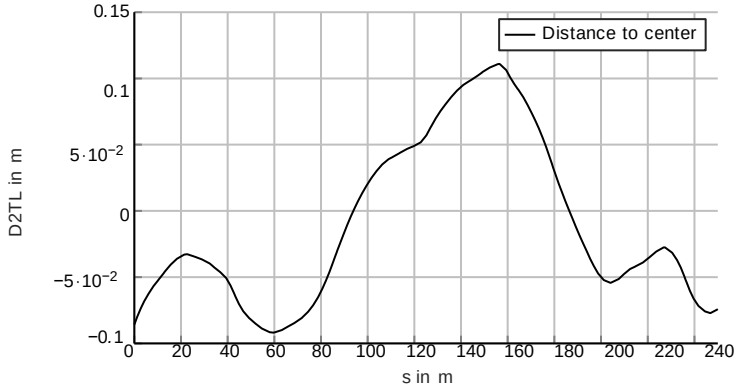

Figure 14: Calculated displacement to lane center.

Based on the localization, the curve-cutting-gradient (CCG) is calculated and represents the stationary driving behavior of the VUT. For all stationary events within the measurement, the average lateral acceleration and distance to center line is plotted. A stationary event is defined as an area in which the standard deviation of the lateral acceleration is less than 10% and for at least 3 s. Additionally, the LKAS needs to be activated during the event. Using a linear regression, the slope of the point-cloud is calculated. Even if the slope is greater than zero, the VUT actively cuts the curve, whereby a negative CCG (which conforms the slope of the linear regression) means that the VUT drifts out of the curve while driving with activated lane keeping assistant. A horizontal slope represents a centered VUT. An example of the CCG-graph ($CCG = -0.06\ \mathrm{m}/\frac{\mathrm{m}}{\mathrm{s}^2}$) is given (Figure 15).

This KPI is also an indicator for the predictability and accuracy of the LKAS controller. The smaller the jitter, the more accurate and predictable the LKAS is. Jitter is defined as the area where 90% of all points are located. Therefore, it automatically estimates the area meeting this criterion. The graph shows also a general positioning offset during a straight drive.

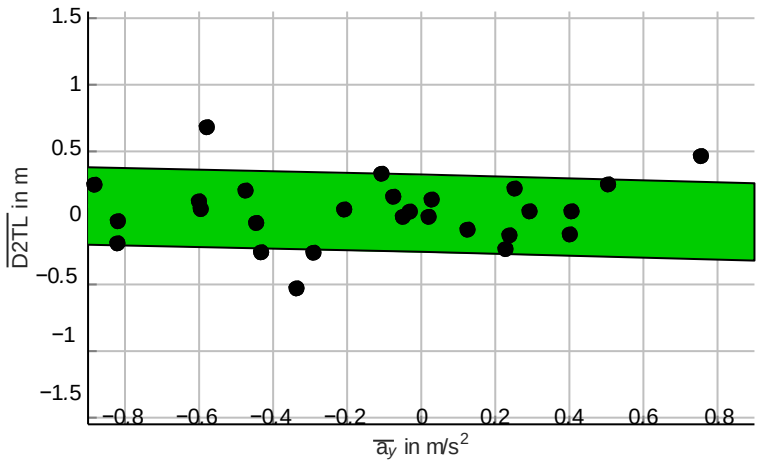

Figure 15: Curve-cutting-gradient as KPI.

7 Practical application for steering assistance

As well as its application in post processing validation methods, GT data can also be used directly within the driver assistance function itself as a virtual sensor. Since some road features are hard to detect with conventional sensors, it makes sense to extend the environment perception with position related road attributes.

To support the human driver, lateral assistance systems calculate an additional steering torque based on the current road visual perception in order to keep the vehicle safely on track. As shown in [21], in addition to the current road curvature and vehicle displacement, the road bank angle q_t significantly impacts the quality of the lane keeping controller. To compensate for this effect, in [22] a novel spatiotemporal end-to-end trained multi fusion steering model is proposed. The objective is to reproduce a demonstrated human steering behavior in real world driving. The network input X_t consist of the raw pixel stream of a front facing RGB camera I_t, selected vehicle signals S_t and the predicted road bank angle gradient vector $\dot{Q}_t$. The steering rack position z_t is proportional to the steering angle δ_t and defines the network output Y_t. A brief visual overview of the model is presented (Figure 16).

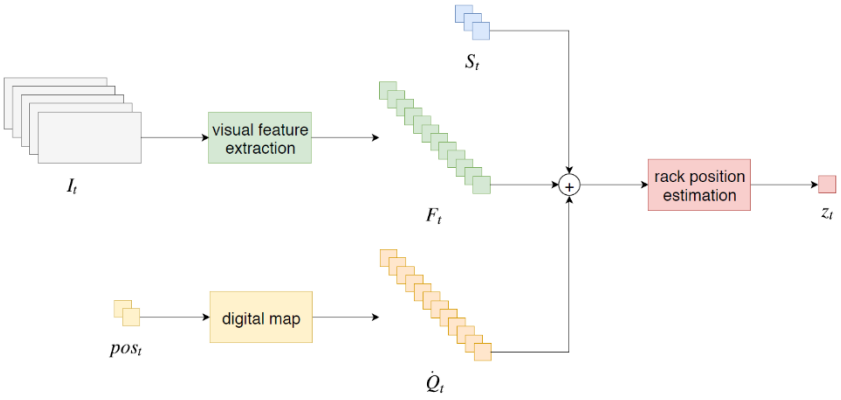

Figure 16: Global overview of the multi fusion end-to-end trained steering model [22]. A defined number of camera frames are bundled within It, and $\dot{Q}t$ defines the vector of predicted road bank angle changes based on location related map data. The vehicle signals are grouped within St.

$\dot{Q}_t$ forms a preview of bank angle changes, referencing the current angle q_t, with a preview vector length of ω_q and the temporal granularity of s_q:

$$\dot{Q}_t = (\dot{q}_t, \dot{q}_{t+s_q}, \ldots, \dot{q}_{t+s_q(\omega_q-1)}) \tag{4}$$

Due to the road description within a distance-related, equidistant grid, these values can easily be derived in realtime based on the current corrected vehicle location pos_t, its velocity v_t and acceleration a_t. For this purpose the CRO Layer one is used and a_t is assumed to be constant in a simplified manner.

Results show that, compared to a merely visual system, the inclusion of road bank angle gradients results in a performance gain of eight percent. In addition, human related pendulous steering errors are compensated, which leads to a smoother driving behavior of the Deep Neural Network based steering controller. The final multi fusion steering model is characterized by an inference performance of 69 frames per second on an automotive computing platform and achieves a minimal mean squared error of 0.0038 mm^2.

8 Visual Range Finder

A Visual Range Finder (VRF) is a device that measures angle and distance from the observer to a target using a camera sensor. The standalone VRF application is to find relative localization, meaning, knowing the initial pose, and estimate the current target pose. In order

for the VRF device to identify the visual object and localize the position, the device should have high computation power for image processing and a large data bank to match visual objects. This makes VRF device to have a large memory, high processing CPU and a larger storage space. This section explains the benefits of using CRO maps by the VRF device.

The system solution includes the DGPS, the CRO maps and VRF. The DGPS data accuracy vary with environmental conditions and provide the probable boundary to VRF. The VRF obtains required data from CRO map that is sufficient enough to compute ahead the expected visual frame boundaries. Knowing visual frame boundaries in advance enables VRF to perform calculations with less data and less computation power.

The VRF device which relies on image processing for identifying landmarks benefits from CRO maps in the following ways:

- Road stripes and lane information in CRO maps helps VRF to localize at high frequency thereby minimizing the time period of error accumulation and increasing robustness of the system (CRO layer 1).
- The anticipated landmark classification is obtained in advance by CRO maps, thereby reducing VRF module classification time from large range of possibilities to one or two classification (CRO layer 2).
- Knowing the current coordinates and landmark coordinates, the visual region of interest is calculated. Since VRF process only ROI, the performance is increased (CRO layer 2).
- The CRO maps has the deep learned key descriptor layer of landmarks, which increases the accuracy of VRF in identifying the landmarks and reduces dependency on the landmarks physical attributes (CRO layer 2).
- The key descriptor layer design allows the system to upgrade CRO maps online or offline, with less or no change to the VRF module. Thus reduces the maintenance of VRF device (CRO layer 2).

9 Conclusion

In order to test and further develop ADAS, high-precision GT maps are required. This paper has shown that a localization of a vehicle position in the CRO maps is $< \pm 0.05$ m accurate. Thus important KPIs for the evaluation of current LKAS can be determined. On the one hand these

serve the safety of ADAS. On the other hand, the performance of ADAS can be increased. In the future, research will continue on the GT approach, as the CRO data format can be easily extended. Depending on the requirements, further layers will be developed and used for AD. Currently, there are also other projects such as the parking assistant, which requires highly accurate environmental information. In the long term, the use of HD maps is essential for AD and its development.

10 Outlook

Another area of application for GT maps is the evaluation of sensor performance. Many sensors in the context of ADAS require an accurate reference of the road. The LKAS camera is such a sensor. The curvature is suitable for evaluating camera performance. The determined curvature of the road is compared with the GT curvature (Figure 17).

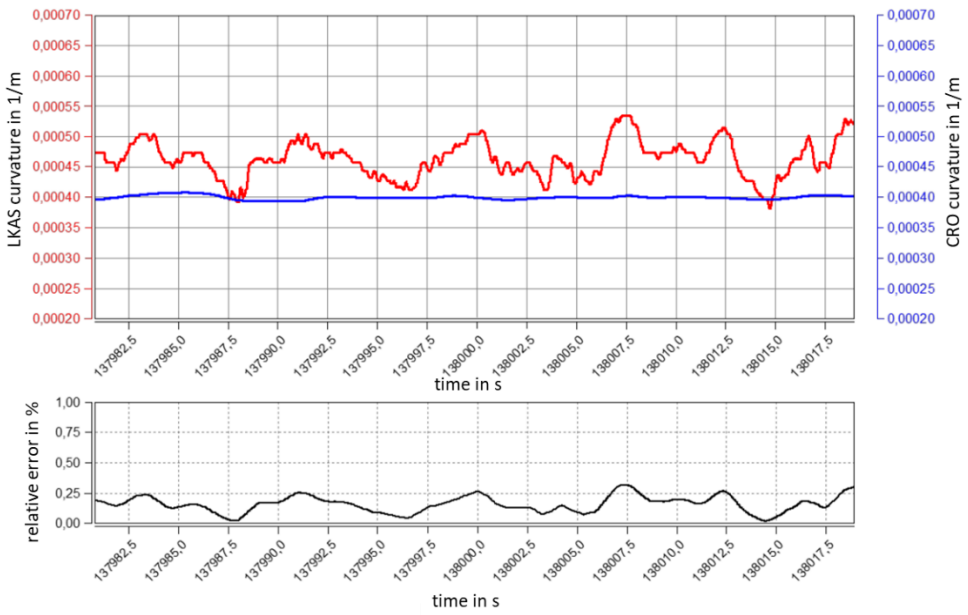

Figure 17: Comparison of GT curvature (blue) to LKAS curvature (red) with relative errors (black).

The red signal of the LKAS camera shows considerable variations compared to the GT road curvature. Relative errors more than 30 % could be observed. This shows considerable potential for improvement in the detection of road markings and the calculation of road parameters.

References

[1] B. Schick, C. Seidler, S. Aydogdu, and Y.-J. Kuo, “Fahrerlebnis versus mentaler Stress bei der assistierten Querführung”, *ATZ-Automobiltechnische Zeitschrift*, vol. 121, no. 2, pp. 70-75, 2019.

[2] B. Schick, F. Fuhr, M. Höfer, and P. E. Pfeffer, “Eigenschaftsbasierte Entwicklung von Fahrerassistenzsystemen”, *ATZ-Automobiltechnische Zeitschrift*, vol. 121, no. 4, pp. 70-75, 2019.

[3] A. Bartels, M. Rohlfs, S. Hamel, F. Saust, and L. K. Klauske, “Lateral guidance assistance”, *Handbook of Driver Assistance Systems: Basic Information, Components and Systems for Active Safety and Comfort*, pp. 1207-1233, 2016.

[4] Euro NCAP, “EUROPEAN NEW CAR ASSESSMENT PROGRAMME (Euro NCAP)”, *October*, no. October, 2018.

[5] UNECE, *Unece r79: Ece/trans/wp.18/2018/10*, 2018.

[6] R. Matawa and O. Vaculín, “Bewertung und Absicherung von Fahrerassistenzsystemen”, *ATZextra*, vol. 21, no. 8, pp. 20-23, 2016.

[7] K. Talmi and O. Jaenisch, “Basis für das automatisierte Fahren-Intelligente Test-und Validierungslösungen”, *ATZelektronik*, vol. 14, no. 3, pp. 16-21, 2019.

[8] S. M. Keidler, “Entwicklung fahrstreifengenauer Ground Truth Karten zur objektiven Verhaltensanalyse von automatisierten Fahrfunktionen unter Echtzeitbedingungen”, Master’s thesis, 2019, p. 81.

[9] various, “OpenCRG UserManual”, [Online]. Available: https://www.vires.com/opencrg/docs/1.1.rc1/OpenCRGUserManual.pdf.

[10] D. Schneider, H. Lategahn, B. Huber, and B. Schick, “Measuring method for function and quality of automated lateral control based on high-precision digital ”ground truth” maps”, in *VDI-Berichte 2335*, 2018.

[11] W. Strijbosch, “Sicheres autonomes Fahren mit hochauflösenden Karten”, *ATZ-Automobiltechnische Zeitschrift*, vol. 120, no. 11, pp. 28–35, 2018.

[12] Dominique Bonte and James Hodgson, “THE FUTURE OF MAPS: TECHNOLOGIES, PROCESSES, AND ECOSYSTEM”, *ABI Research*, vol. 2018, 2018. [Online]. Available: https://www.here.com/file/7766/download?token=dwOqPUix.

[13] K. Massow, B. Kwella, N. Pfeifer, F Häusler, J. Pontow, I. Radusch, J. Hipp, F. Dölitzscher, and M. Haueis, “Deriving hd maps for highly automated driving from vehicular probe data”, in *2016 IEEE 19th International Conference on Intelligent Transportation Systems (ITSC)*, IEEE, 2016, pp. 1745-1752.

[14] S. F. Wiesbaden, “Das antizipierende Automobil”, *ATZextra*, vol. 22, no. 3, pp. 8-11, 2017.

[15] Marius Dupuis, “OpenDRIVE Manager: User Manual”, [Online]. Available: https://vires.com/download/OpenDRIVE/OdrMgrUserManualRevI.pdf.

[16] J. Inman, *Navigation and Nautical Astronomy for the Use of British Seamen*. C. and J.Rivington, 1835. [Online]. Available: https://books.google.de/books?id=-fUOnQEACAAJ.

[17] T. Vincenty, “Direct and inverse solutions of geodesics on the ellipsoid with application of nested equations”, *Survey Review*, vol. 23, no. 176, pp. 88–93, 1975. DOI: 10.1179/sre.1975.23.176.88.

[18] G. E. GmbH, *Adma 3.0 technical documentation*, GeneSys Elektronik GmbH.

[19] M. E. McCauley and T. J. Sharkey, “Cybersickness: Perception of self-motion in virtual environments”, *Presence: Teleoperators and Virtual Environments*, vol. 1, no. 3, pp. 311-318, 1992, ISSN: 1054-7460. DOI: 10.1162/pres.1992.1.3.311.

[20] ISO, *Mechanische Schwingungen und Stöße - Bewertung der Einwirkung von Ganzkörper-Schwingungen auf den Menschen - Teil 1: Allgemeine Anforderungen*, 1997.

[21] D. Heide and A. O. Ag, “Banked road estimation and compensation algorithm for Lane Keeping Assist and its integration in GM ’ s Software Architecture”, pp. 38-42, 2017.

[22] J. Haselberger, B. Schick, and J. Chen, “Deep Learning for lateral vehicle control - An end-to-end trained Multi Fusion steering model”, in *10th International Munich Chassis Symposium 2019*, 2019.